

CFD simulation of wind-driven inter-unit dispersion around multi-storey buildings: upstream building effect

Y.W. Dai¹, C.M. Mak¹, Z.T. Ai²

¹ Department of Building Services Engineering, The Hong Kong Polytechnic University, Hong Kong, China

² International Centre for Indoor Environment and Energy, Department of Civil Engineering, Technical University of Denmark

Corresponding author: C. M. Mak, Department of Building Services Engineering, The Hong Kong Polytechnic University, Hung Hom, Kowloon, Hong Kong. Email: cheuk-ming.mak@polyu.edu.hk

Abstract

Previous studies on inter-unit dispersion around multi-storey buildings focused mostly on an isolated building. Considering that the presence of an upstream building(s) would significantly modify the airflow pattern around a downstream building, this study intends to investigate the influence of such changed airflow patterns on inter-unit dispersion characteristics around a multi-storey building due to wind effect. CFD method in the framework of Reynolds-averaged Navier-stokes modelling was employed to predict the

coupled outdoor and indoor airflow field, and the tracer gas technique was used to simulate the dispersion of infectious agents between units. Based on the predicted concentration field, a mass conservation based parameter, namely re-entry ratio, was used to evaluate quantitatively the inter-unit dispersion possibilities and thus assess risks along different routes. The presence of upstream building(s) could disrupt the strong impingement of approaching flows but brings a more complex and irregular airflow pattern around the downstream multi-storey buildings, leading to a more scattered distribution of re-entry ratio values among different units and uncertain dispersion routes. Generally, the tracer gas concentration in most units were lower than those in an isolated building, although very high concentrations were found in some specific areas.

Keywords

CFD, inter-unit dispersion, ACH, natural ventilation, infectious risk assessment

Introduction

Natural ventilation through windows is a convenient and sustainable ventilation strategy to induce air exchange to cool the overheated indoor air and dilute the contaminated air in residential buildings¹⁻³. However, apart from bringing in fresh air from outside, this approach could also cause incursion of outdoor pollutants into the interior area⁴, which include traffic exhausts, dusts, and pollens⁵, as well as airborne transmitted virus, such as severe acute

respiratory syndrome (SARS)⁶. There have been reports given by research papers⁶⁻⁸ illustrating cross transmission between apartment units (so-called inter-unit dispersion) as a valid airborne transmission route of infectious diseases. Thus, understanding these mechanisms and routes of cross transmission would be essential to control dispersion and ventilation of pollutants in buildings.

A substantial body of former research conducted on the airflow field and pollutant dispersions around buildings forms the foundation for the present study. On-site measurements, wind tunnel experiments and numerical simulations have been carried out regarding the inter-unit dispersion. Li et al.^{6,8} identified the inter-unit dispersion as an important airborne transmission route after the outbreak of SARS epidemic in 2003 in Amoy Gardens housing by CFD method and multi-zone modelling. Niu and Tung⁹ adopted on-site tracer gas technique to examine the pollutant transportation paths through windows which was primarily driven by buoyance effect caused by the air temperature difference between indoor and outdoor environments. They found that the re-entry ratio of the gaseous pollutant from a lower unit to an immediate upper unit can reach up to 7%, which was equivalent to about 2% infectious risk based on the Wells-Riley infection risk assessment model⁷. However, this work was limited to two upper-lower floors. Liu et al.^{10,11} and Wang et al.¹² performed wind tunnel experiments to investigate the wind effect on the pollutant dispersion around a complicated cross shape (#) building, as illustrated in Figure 1. The pollutant was found to travel along both upward and downward direction to re-enter into units, as well as

horizontal dispersion. However, only a specific geometry of the building was investigated in their research. More recently, a wind tunnel experiment with a generic shape multi-storey building was carried out by Mu et al.^{13, 14} Their research investigated the inter-unit pollutant transmission using the tracer gas method, examining the effect of wind direction and source location. The re-entry pollutant concentration was calculated under assumed circumstances to assess the infection probability of each unit. However, these two wind tunnel experiment studies were both limited to an isolated building. Further, the wind tunnel tests may not be able to consider the indoor airflow field correctly due to the similarity problem.

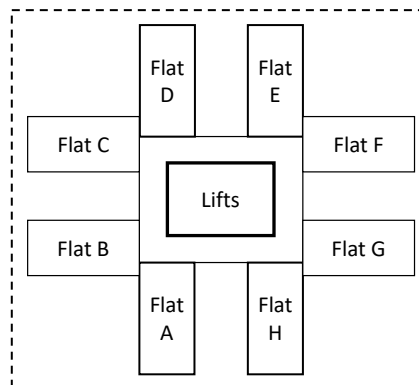


Figure 1. Schematic plan view of the cross shape (#) building.

Some recent studies¹⁵⁻¹⁷ have shown that CFD approach is specifically suitable for the investigation of natural ventilation and becomes the most widely used model. Gao et al and Liu et al.^{18, 19} investigated the CFD simulations of an on-site measurement⁹ to quantify the infection risks. Ai et al.²⁰⁻²³ studied the inter-unit dispersion characteristics of gaseous

pollutant in and around two hypothetical envelope buildings under wind-induced single-side ventilation by CFD method. The tracer gas transmission mechanism on the windward and leeward sides was presented and compared with that of cross shape (#) buildings. The results showed that inter-unit dispersion pattern was highly dependent on the wind direction and the re-entry ratio of gaseous pollutants can reach up to 10%. However, these previous studies were limited to an isolated building with a slab-like shape. Recently, Cui et al.²⁴ numerically calculated the inter-unit re-entry ratios of a cylinder shape building under the influence of an upstream interfering building. The results showed that the presence of an upstream building changed the airflow characteristics and pollutant transportation routes dramatically. However, the work by Cui et al.²⁴ considered only a single upstream building and a limited number of windward side source locations of the target building.

One of the main purposes of natural ventilation in residential buildings is to dilute air pollutant in order to improve the indoor air quality. Many studies have been conducted to reveal the natural airflow patterns. However, in real urban areas, an isolated building is rare, most of buildings are surrounded by many others. An isolated building or a specific shape of a building cannot be used for better prediction in an actual urban environment. Therefore, the present work aims to investigate airflow characteristics and pollutant dispersion in a more realistic situation of the urban environment.

The present study focuses on the inter-unit dispersion characteristics of gaseous pollutants within a cylinder-like multi-storey building under the effect of two upstream buildings based on computational fluid dynamics. The upstream buildings with generic shape are set to better analyse the real urban environment. The two upstream buildings and the target building are intended to represent a basic building group in an actual urban environment, which serves to provide the basic airflow fields for the investigation of inter-unit dispersion. The buoyancy-driven pollutant transmission has been reported to be caused by a common indoor-outdoor temperature difference, investigated in previous studies^{9, 18}. The airflow carrying the pollutant is unidirectional, namely upward, and only important in relatively low wind speed conditions (lower than 0.9 m/s). In urban environments, wind speeds can be easily over 0.9 m/s . Therefore, this present study only considers the isothermal airflow, which is driven by wind effect and leads to more diverse dispersion routes and re-entry ratios. Given that the airflow pattern and pollutant dispersion around buildings could be significantly affected when occurring under different prevailing wind directions, the approaching wind angle is considered as one of the key factors in the research. Tracer gas technique, carbon dioxide (CO_2), is adopted to simulate the gaseous pollutant in the present study, owing to the similarity of its aerodynamics characteristics to those of various gaseous pollutants and fine particles. The results of this research are expected to be useful in understanding the pollutant dispersion mechanism in urban environment and in developing effective strategies for the control of infectious respiratory diseases.

CFD methods and model validation

Turbulence models

The CFD approach has been commonly used to predict airflow patterns and pollutant dispersions in and around buildings. The two-equation Reynolds-averaged Navier-Stokes (RANS) models with standard $k - \varepsilon$ turbulence model²⁵ and its modifications^{26, 27} maintain the most widely used turbulence model to solve wind engineering and atmospheric dispersion problems²⁸. Turbulence effects in this study are taken into consideration by using renormalization group (RNG) $k - \varepsilon$ model²⁹, and two near-wall treatment methods are applied to model the airflow in the near-wall regions. For incompressible flow, the time-averaged governing equations can be written generally as Equation (1):

$$\frac{\partial}{\partial t}(\varphi) + \nabla \cdot (\bar{u}_\varphi) = \nabla \cdot (\Gamma_\varphi \nabla \varphi) + S_\varphi \quad (1)$$

where φ represents the scalars: the velocity ingredients u (m/s), v (m/s), w (m/s), the turbulent kinetic energy k (m^2/s^2), its dissipation rate ε (m^2/s^3), and the mass fraction M_i (g/m^3); term \bar{u} (m/s) the mean velocity, Γ_φ the effective diffusion coefficient for each variate, and S_φ the source term.

The RNG $k - \varepsilon$ model offers a number of improvements over the standard $k - \varepsilon$ model, which presents an authentic interrelation between the turbulence transport and

Reynolds number by a more precise differential equation. This allows the RNG model to have superior performance in predicting the low-Reynolds-number and near-wall flows. Further, an additional strain-dependent term, R_ε , in the transport equation for ε makes the RNG model with high sensitivity over dealing with rapid strain and streamline curvature than the standard $k - \varepsilon$ model. The added term R_ε is shown by Equation (2), as:

$$R_\varepsilon = \frac{C_\mu \rho \eta^3 (1 - \eta/\eta_0)}{1 + \xi \eta^3} \cdot \frac{\varepsilon^2}{k} \quad (2)$$

where C_μ , η_0 and ξ are model constants, and $\eta \equiv Sk/\varepsilon$ where S is the scale of strain rate. A more detailed demonstration of the RNG model and its empirical values are offered in Fluent (2010).

The governing equations of numerical models are discretized into algebraic equations on a staggered grid system with the finite volume method.

Description of the wind tunnel experiment

In the present study, a wind tunnel experiment conducted at the University of Hamburg³⁰ was used to validate the RANS models and near-wall treatments. Airflow and dispersions around a finite array of rectangular building models (CEDVAL B1-1) were measured at a reduced scale of 1:200 in the Blasius wind tunnel. The experiment model included 3×7 array of buildings

with four facing pollutant sources located on the leeward side of one target building, the physical configuration of which is shown in Figure 2. The high-quality experiments were conducted with the boundary layer flow which has been validated by full-scale data in the test section before the building model was set up. Some locations on five planes were measured in the experiment: four vertical planes at $Y = -H$, $Y = -0.6H$, $Y = -0.4H$, and $Y = 0$, respectively, and a horizontal plane at $Z = 0.5H$. The Laser Doppler Velocimetry (LVD) technique was adopted to perform the velocity and turbulence fields, and the Flame Ionization Detector (FID) was used to measure the concentration of the pollutant. Noted that k was calculated by the measured fluctuating velocities, $k = 0.5(u'^2 + v'^2 + w'^2)$. The concentration field is presented in a non-dimensional form as given in Equation (3):

$$K_c = \frac{C_{local}}{C_{source}} \cdot \frac{U_{ref} H^2}{Q_{source}} \quad (3)$$

where C_{local} is the measured tracer gas concentration (ppm) with environment background concentration subtracted, C_{source} is the tracer gas concentration (ppm) at the source, U_{ref} is the reference wind speed (m/s) measured at the height of $0.66m$, H is the model building height ($H = 0.125m$) and Q_{source} is the total source strength (m^3/s).

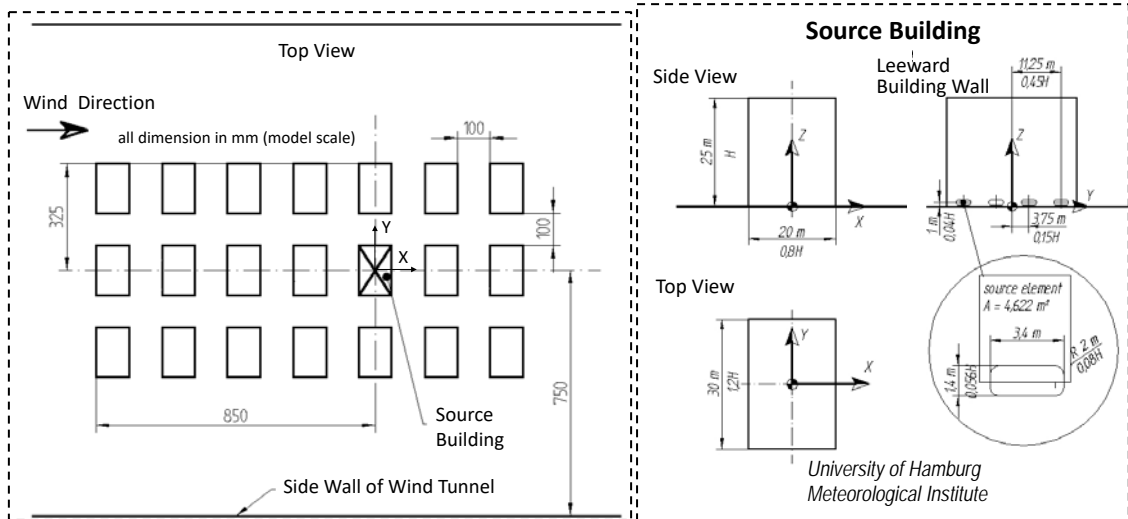


Figure 2. Dimensions of building models, the source building and source emissions in wind tunnel experiment³⁰.

Computational settings and parameters

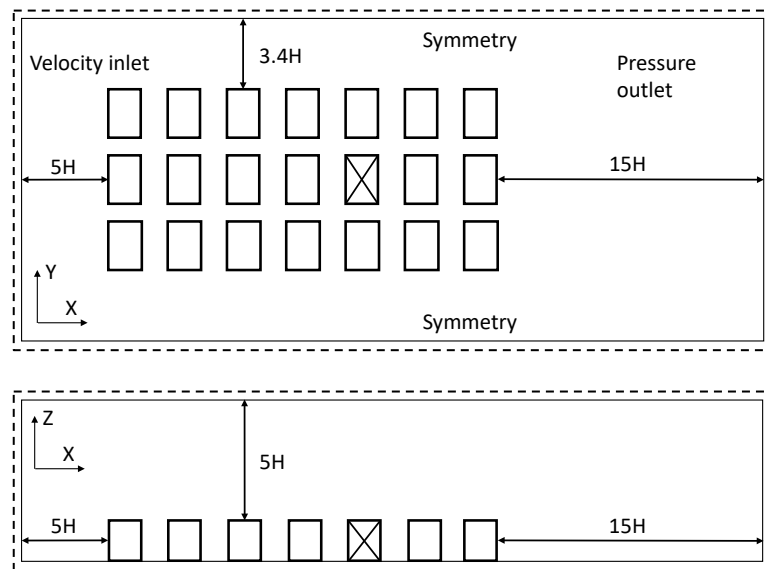


Figure 3. Computational domain: top view and side view.

A computational domain shown in Figure 3 was constructed to simulate the flow and dispersion fields around the building models. This domain size was based on the existing best practice guideline³⁸, which is spatially large enough to eschew the intervention within the flow development, except for the side width which was built upon the wind tunnel width. The boundary conditions at the domain's inlet, lateral sides, ceiling, and outlet are summarized in Table 1, where the inlet velocity profile follows a power law, by fitting $U = U_H \cdot (\frac{Z}{Z_H})^\alpha$, $U_H = 6m/s$, $Z_H = 0.5m$ and $\alpha = 0.21$. In addition, the Von Karman constant κ is 0.4187 and $C_\mu = 0.069$ ^{31, 32}. When the dispersion was simulated, the tracer gas (CO_2) was uniformly released from the four source elements (see 2) with a constant velocity of $0.025m/s$ in the X direction.

Table 1. Boundary conditions

	Power law type
Domain inlet	$U = U_H (\frac{Z}{Z_H})^{0.21}$ $k = 0.5(u'^2 + v'^2 + w'^2)$ $\varepsilon = C_\mu^{0.75} k^{1.5} / l$
Domain outlet	$\frac{\partial}{\partial x}(u, v, w, k, \varepsilon) = 0$
Domain ceiling	$w = 0, \frac{\partial}{\partial x}(u, v, k, \varepsilon) = 0$
Domain lateral sides	$v = 0, \frac{\partial}{\partial x}(u, w, k, \varepsilon) = 0$
Domain ground	Standard wall functions and enhanced wall functions
Building surfaces	Non-slip for wall shear stress
Turbulence model coefficients	$C_\mu = 0.069, \kappa = 0.4187$

A comprehensive mesh test was conducted for the dependence of numerical solutions on grid number. Three mesh systems with approximately 5.4, 6.0 and 6.7 million grids of structured

hexahedral cells were created and compared (see Figure 4(a)), in which the medium one was selected because of the compromise between numerical accuracy and cost. Two near-wall treatment methods were compared.

The first method is the standard wall functions in which the near wall y^+ is around 35, the minimum grids widths near the domain ground and building walls are 0.005m. Another is the enhanced wall functions³³. The enhanced wall functions divide the whole domain into a viscosity-affected and a fully-turbulent region, where the former is resolved by a one-equation model and the latter by the two-equation $k - \varepsilon$ model. The minimum grids widths near the domain ground and building walls are 0.0002m and the near wall y^+ is less than 5. A schematic view of the mesh information can be found in Figure 4(b). Because of the improved resolution of the near-wall regions and a better treatment of the near-wall flows, the enhanced wall functions provide more accurate velocity fields near the domain ground and in the region around the building roof when compared to that given by standard wall functions³³.

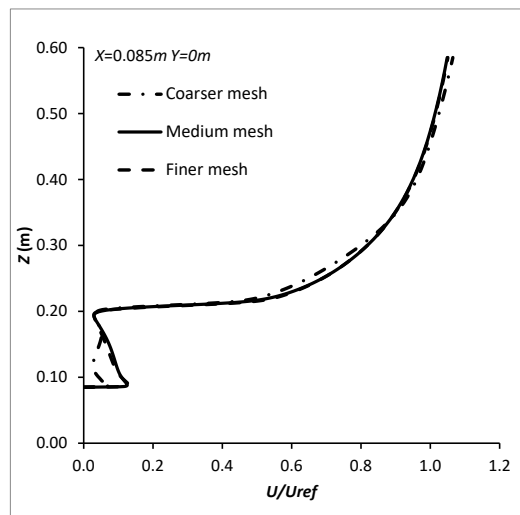


Figure 4. (a) Comparison of mean velocity profiles using three types of mesh systems at the vertical line of $X = 0.085m$.

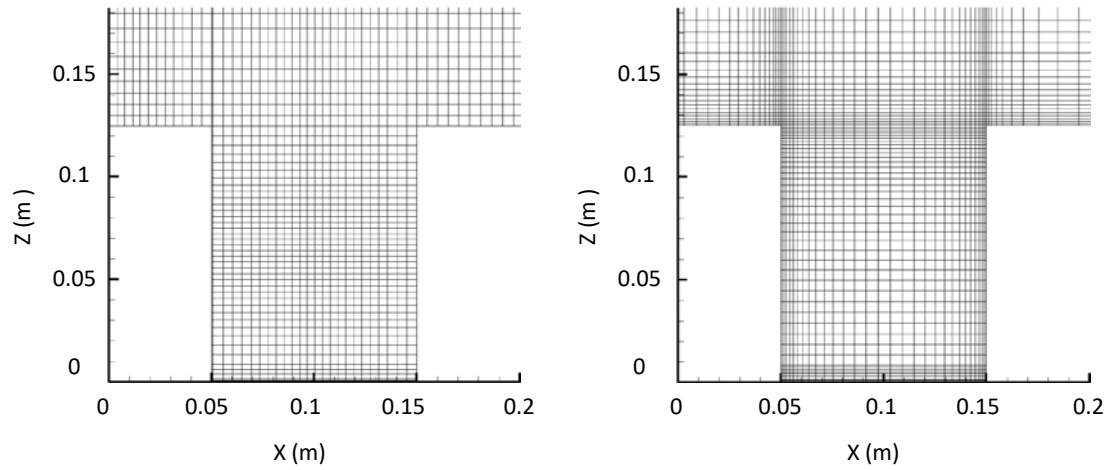


Figure 4. (b) Mesh details for a part of the vertical line of $Y = 0$: the coarser for standard wall functions and the finer for the enhanced wall functions.

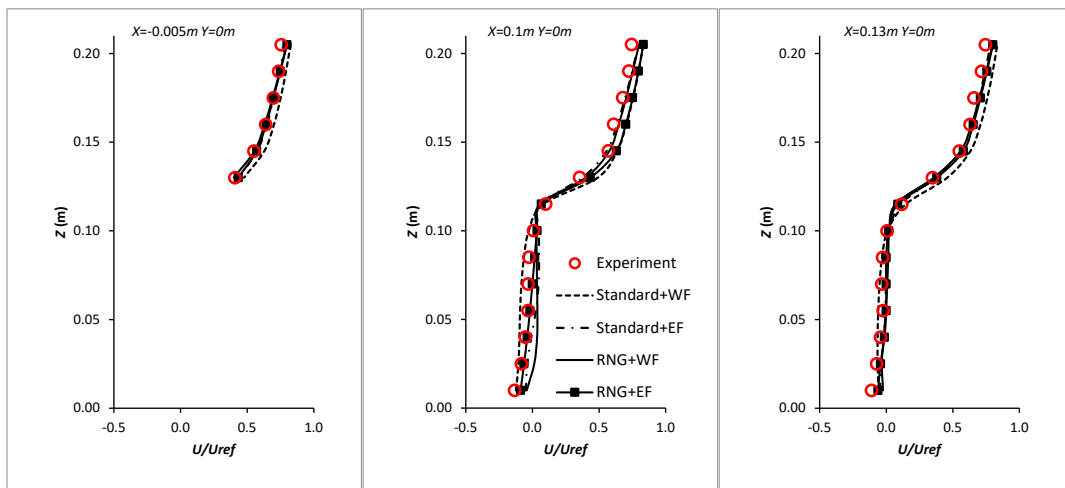
Commercial CFD code ANSYS Fluent 13.0.0³⁴ was used to simulate the wind tunnel model. Four numerical setting combinations were conducted in the validation work, standard $k - \varepsilon$ model plus standard wall functions; standard $k - \varepsilon$ model plus enhanced wall functions; RNG $k - \varepsilon$ model plus standard wall functions and RNG $k - \varepsilon$ model plus enhanced wall functions, respectively. The SIMPLEC algorithm was adopted for the pressure-velocity coupling.

The pressure interpolation is second order accuracy discretization schemes, as well as both the convection and diffusion terms. Convergence is supposed to be achieved when all the

scalar residuals were less than 10^{-6} and the stability of calculation is reached over packs of iterations.

Comparison between experimental and simulated results

The comparison of non-dimensional air velocity distribution of X direction along six vertical lines between the numerical results and wind tunnel data is shown in Figure 5. Compared to the experiment data, the average deviations of velocities produced by these four numerical combinations are 24.85%, 20.75%, 16.31% and 8.48%, respectively. Obviously, the RNG $k - \varepsilon$ model with enhanced wall function produced more accurate airflow results around the target body, except for the slightly larger velocities above the roof of target building model ($Z > 0.15 \text{ m}$). However, this little deficiency can be accepted because the airflow distribution over the building roof ($Z > 0.15 \text{ m}$) is not under the consideration of present study.



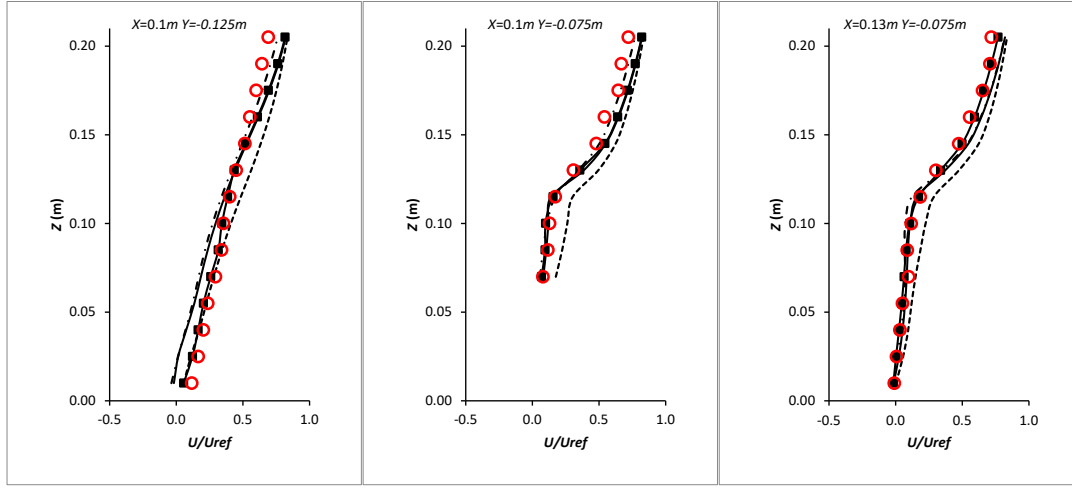


Figure 5. X velocity distribution at the six vertical lines: Standard + WF indicates standard $k - \varepsilon$ model plus standard wall functions; Standard + EF indicates standard $k - \varepsilon$ model plus enhanced wall functions; renormalization group (RNG) + WF indicates RNG $k - \varepsilon$ model plus standard wall functions; RNG + EF indicates RNG $k - \varepsilon$ model plus enhanced wall functions.

Based on the RNG $k - \varepsilon$ model and enhanced wall function, the air pollutants were released to predict the concentration field. The turbulent Schmidt number (Sc_t), which is defined as the ratio of turbulent momentum diffusivity to concentration (tracer gas) diffusivity, performs an essential influence on the calculation of concentration equation in the simulation with RANS models³⁵. The specific value of Sc_t has a significant effect depended on dispersion problems and flow structures and the optimum values of this number are distributed in the range of 0.2-1.3^{35, 36}. In the present study, the value of 0.7 was used and it

shows good agreement of concentration field between numerical simulation data and wind tunnel results. The non-dimensional concentrations of tracer gas K_c at the measured positions are shown in Figure 6.

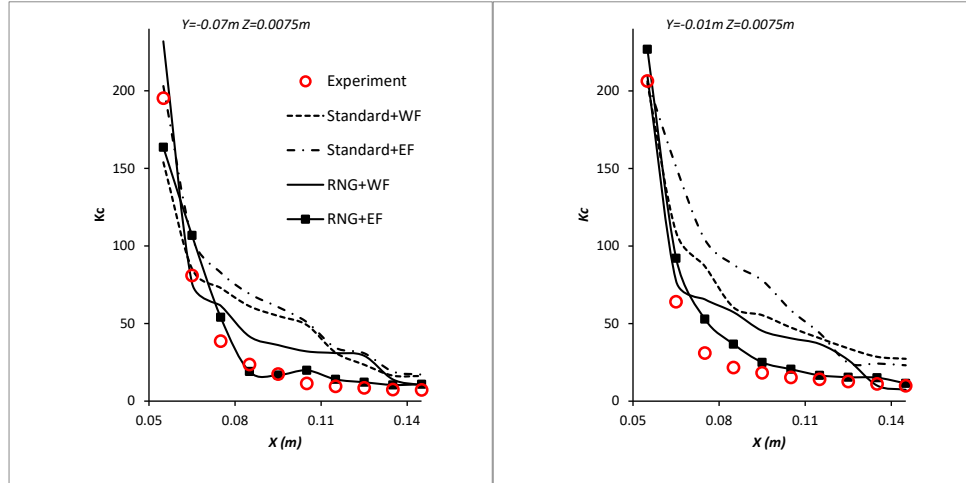


Figure 6. Tracer gas concentration at two horizontal lines: Standard + WF indicates standard $k - \varepsilon$ model plus standard wall functions; Standard + EF indicates standard $k - \varepsilon$ model plus enhanced wall functions; renormalization group (RNG) + WF indicates RNG $k - \varepsilon$ model plus standard wall functions; RNG + EF indicates RNG $k - \varepsilon$ model plus enhanced wall functions.

Overall, this validation justifies the adoption of the selected numerical models (RNG $k - \varepsilon$ model and enhanced wall functions) in the later simulations of the airflow distribution and inter-unit dispersion field around the target building.

Configuration descriptions

In order to investigate the effect of upstream buildings on the wind-induced inter-unit dispersion around a multi-storey building in an urban environment, a 1:20 reduced scale³⁷ downstream building and two upstream interfering buildings were adopted. The building dimensions in the work of Cui et al.²⁴ were used in this present work. Two rectangular models without openings were employed as upstream interfering buildings, as shown in Figure 7(a). The target building has two independent units on each storey with opposite window opening directions, shown in Figure 7(b). The unit dimensions are: width (D_X) \times length (D_Y) \times height (D_Z) = $6m \times 3m \times 3m$, and the window: width (D_X) \times height (D_Z) = $1m \times 2m$, in the prototype. The window bottom is $1m$ above each storey. The target building has 4 storeys. The dimension of width (D_X) \times length (D_Y) \times height (D_Z) = $6m \times 6m \times 12m$. Due to the juxtaposition of the two upstream buildings, the distances of the three buildings are equal to the width of the building, the arrangement is shown in Figure 8(a). The upstream building in front of the target building was named as Building A, and the other was Building B. The distance between two building models is smaller than the leeward recirculation length²⁴.

In order to reproduce the original full-scale flow, a series of similarity criteria including geometry similarity, boundary layer flow similarity and Reynolds independence would be needed to be achieved. The computational domain for all the cases is depended on the best practice guidelines³⁸, as shown in Figure 8(a), an upstream distance of $5D_Z$, downstream distance of $15D_Z$, lateral distance of $6D_Z$ and height of $6D_Z$ were chosen to simulate the natural ventilation, which is large enough to achieve the accurate airflow

distribution. The Reynolds number Re ($Re = V_{ref} \cdot D_z / \nu$) at the top of the building roof in the present study is 40,000 and is much larger than the recommended value, a threshold of 15,000³⁹, which means the Reynolds independence is fulfilled.

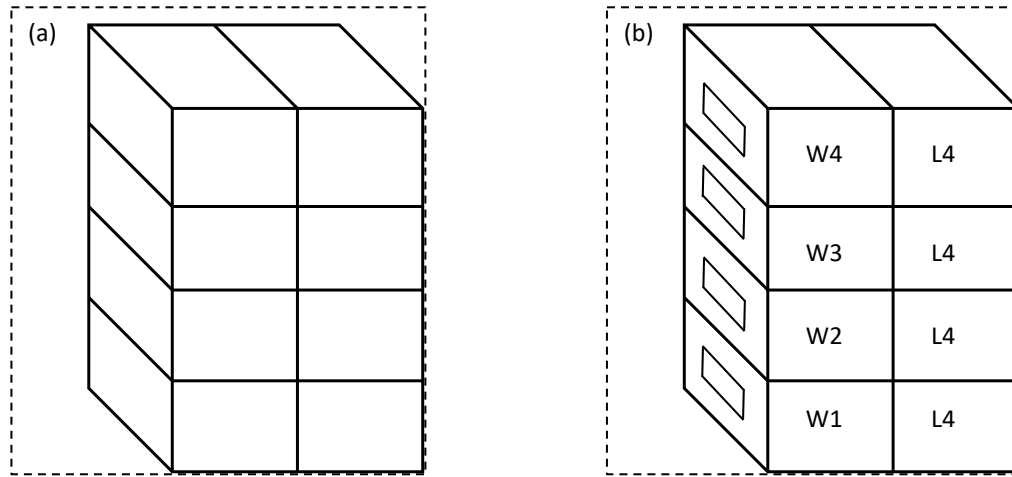


Figure 7. (a) physical model of upstream buildings; (b) physical model of the target building.

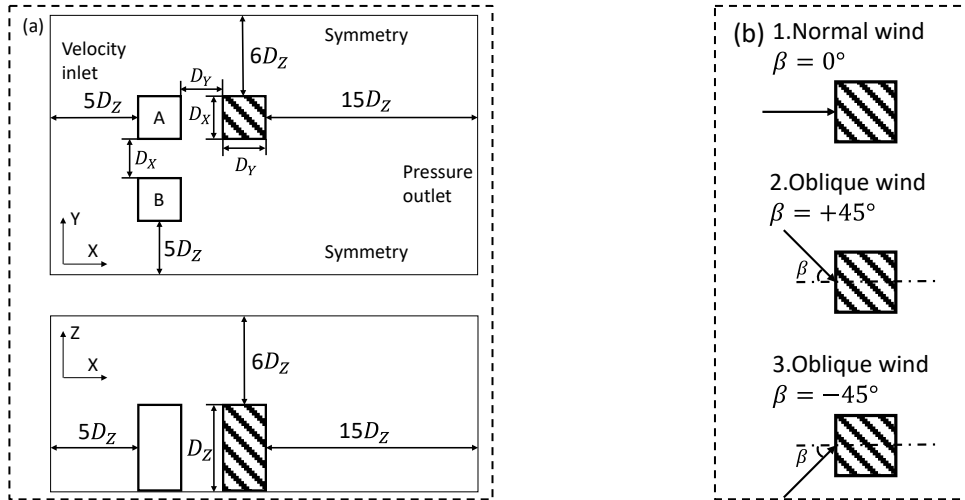


Figure 8. (a) the arrangement and computational domain of three buildings; (b) three wind directions.

The present study selects three wind directions, as shown in Figure 8(b); β is the angle between the incident wind direction and perpendicular to the building surface. The wind at the inlet of computational domain in an urban environment follows a power law profile satisfying Equation (4):

$$V_z = V_{ref} \left(\frac{Z}{Z_H} \right)^\alpha = 1.14 V_{ref} Z^{0.25} \quad (4)$$

where Z_H is the building height ($Z_H = 0.6m$), V_{ref} is the wind velocity at the height of building roof ($V_{ref} = 4m/s$). The turbulence at the inlet boundary is characterized by turbulent intensity and length scale, which are 8% and 1m, respectively. A mesh with 6.0 million grids is employed after a mesh sensitivity test similar to that was described in the validation section. Air exchange rate (ACH) of each unit was calculated by an integral method, as given by Equation (5)^{40, 41}:

$$ACH = 3600 \times \frac{0.5 \int_0^A |V_x| dA}{Vol_R} \quad (5)$$

where V_x (m/s) is the velocity component normal to the plane of the openings, A (m²) is the area of the window, and Vol_R (m³) is the volume of each unit. The tracer gas CO_2 was released at a rate of 8 mg/s in the middle of each unit at a height of 1.6 m. Some

researchers^{9, 21} adopted the re-entry ratio (R_k) to evaluate the inter-unit pollutant dispersion.

The re-entry ratio is defined as the fraction of exhaust air from a source unit i which re-enters into another unit j . It can be calculated by Equation (6)⁹:

$$R_k = M_{i-j} \frac{Vol_j(ACH)_j}{Vol_i(ACH)_i} \quad (6)$$

where M_{i-j} is the mass fraction of concentration that originates from the source unit i ($C_i, kg/m^3$) and is present in another unit j ($C_j, kg/m^3$), which can be calculated as $M_{i-j} = \frac{C_j}{C_i}$. The concentration in a unit is calculated based on the breathing plane (the standing position) at the height of $1.6m$ above the floor. $(ACH)_i$ is the air exchange rate of the source unit and $(ACH)_j$ is the air exchange rate of the re-entry unit.

The units are named as shown in Figure 7(b), in which W indicates the windward side, L the leeward side, and numbers first to fourth storey.

Results and discussion

Airflow characteristics

The airflow distribution in and around a building is essential to affect the airborne transmission of pollutant between units. For an isolated building encountered by urban wind,

the wind would deflect over the top, down in front and around the sides. Because of the air pushing against the building, much of the windward wall would receive a relatively high pressure and the peak pressure would be present at about $2/3$ of the height of the building, where the stagnation zone (the upstream building in Figure 9(a) is under this situation) occurs. When an airflow is influenced by a single upstream building²⁴, air would mainly flow downward near the windward side of the downstream building, causing a recirculation zone near the top of the leeward side of the upstream building, as shown in Figure 9(a). Comparing to a single upstream building, the circumstance under two upstream buildings is different. Figure 9(b) shows the streamlines and mean velocity on the vertical centre plane ($Y = 0$) of buildings under normal wind direction ($\beta = 0^\circ$). When airflow is influenced by two upstream buildings, air would flow downward near the windward side of the downstream building and would cause a small recirculation zone close to the ground. The downward flow and recirculation in the near-wall flow imply that the presence of upstream buildings have considerable effect on the inter-unit dispersion routes, which could cause pollutants to be released from the ground floor and cannot be transported upper ward. Further, under the effect of two upstream buildings, the near-wall airflow on the windward side of the target building would become deviated, thus inducing more low-speed areas.

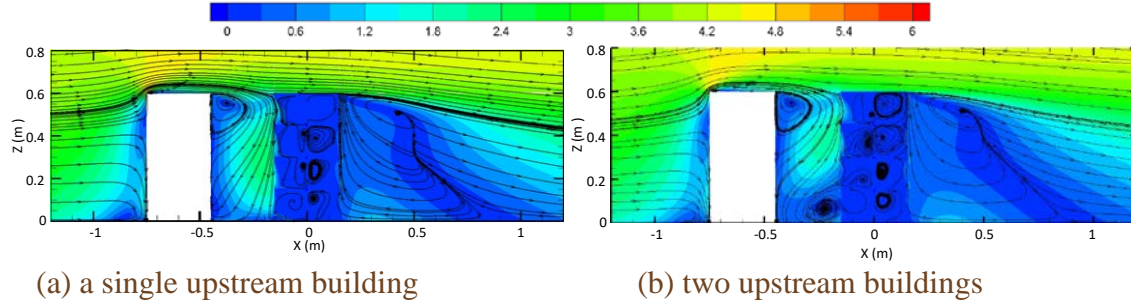
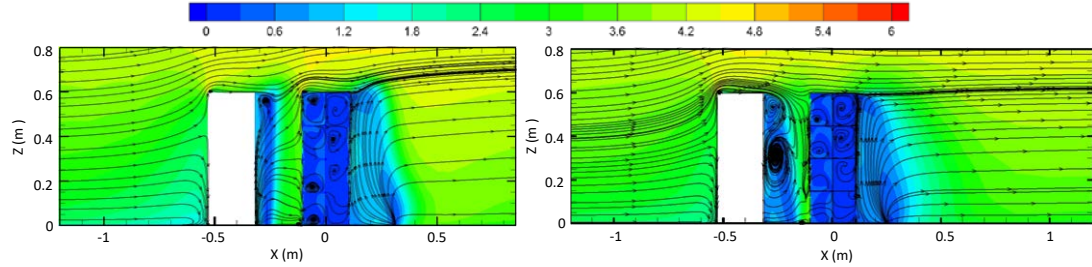


Figure 9. (a) streamlines and mean velocity on the vertical centre plane of a single upstream building ($\beta = 0^\circ$); (b) streamlines and mean velocity on the vertical center plane of two upstream buildings ($\beta = 0^\circ$).

Under the wind direction of $+45^\circ$ ($\beta = +45^\circ$), Figure 10(a) shows the streamlines and mean velocity on the vertical centre plane of the target building. In general, the flow pattern on the windward side is mainly consisted of primarily upward wind and vertical wind, as well as small vortices, while the leeward side is characterized by a strong upward airflow and a small reattachment on the top of the roof, which remains similar to the basic flow pattern under the situation of an isolated building²¹. However, the airflow distribution under the wind direction of -45° ($\beta = -45^\circ$), as shown in Figure 10(b), is dissimilar and characterized by the combination of several strong vortices in the windward side and a substantially upward airflow in the leeward of the target building. When the wind is oblique, the airflow fields are drastically changed because of the upstream buildings, inducing a large high-speed zone in the near-wall area, which implies that the ventilation of the target building is more effective and pollutants disperse more easily under this situation.



(a) vertical centre plane under $\beta = +45^\circ$ (b) vertical centre plane under $\beta = -45^\circ$

Figure 10. Streamlines and mean velocity on the vertical centre plane of the target building under oblique wind directions.

Figure 11(a) shows the airflow path lines on the horizontal plane at the breathing level on the third storey of the target building ($Z = 0.37\text{m}$) with two upstream buildings. In general, for an isolated building, air flows separately into lateral sides under normal wind direction ($\beta = 0^\circ$), causing pollutants released from windward unit to become diluted quickly²⁰. For a single upstream building²⁴, two recirculation zones appear on the windward side of the target building, as shown in Figure 12(a), which is similar to the present study. As mentioned above, a small vortex occurs near the ground on the windward side of target building, which indicates that airflow field may present differently in the lower area. Figure 11(b) shows the airflow streamlines and mean velocity field on the horizontal plane in the middle of the ground floor ($Z = 0.08\text{m}$), comparing to a single upstream building as shown in Figure 12(b), a recirculation zone is formed on the windward side of the target building because of the existence of upstream building B. The airflow field near the target building

would become deviated due to the asymmetry arrangement of the building group, which leads to larger wind speed near the lateral side and diverse pollutant transported routes.

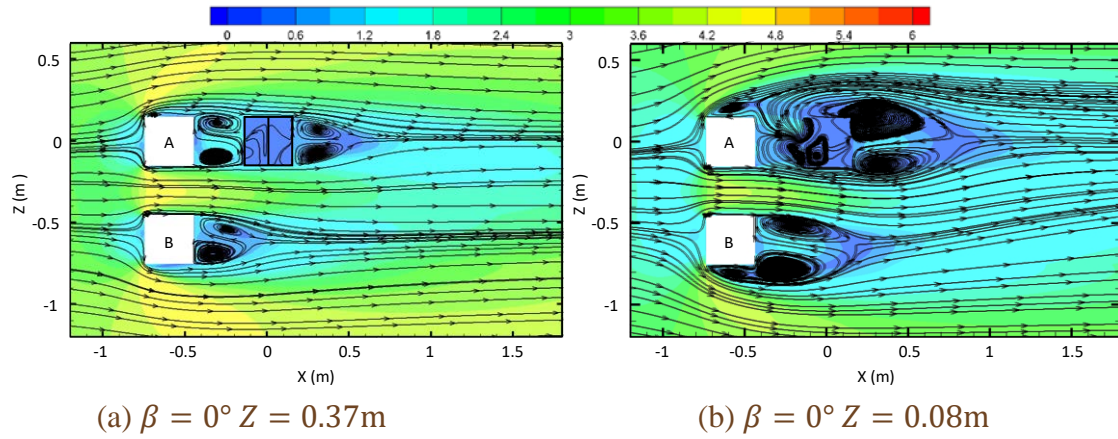


Figure 11. Streamlines and mean velocity on horizontal planes of the target building under different heights with two upstream buildings.

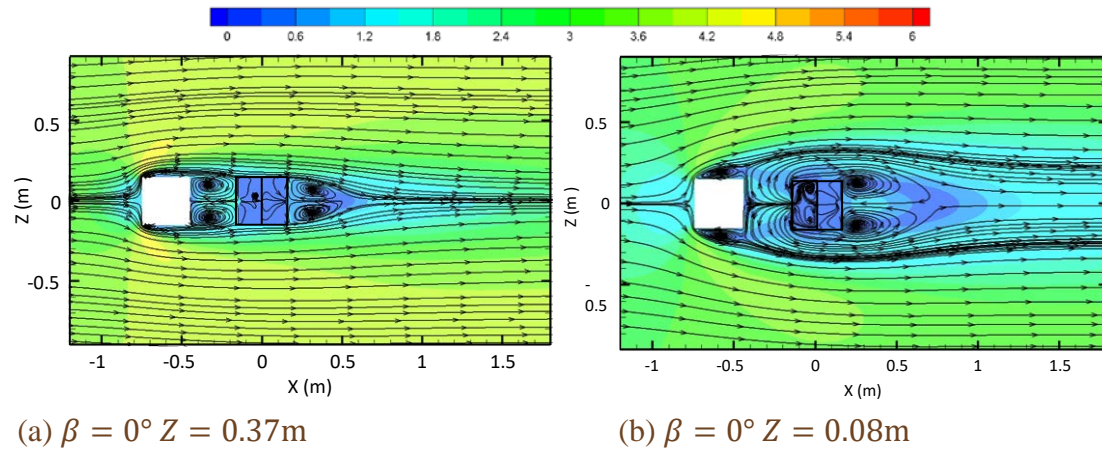


Figure 12. Streamlines and mean velocity on horizontal planes of the target building under different heights with a single upstream building.

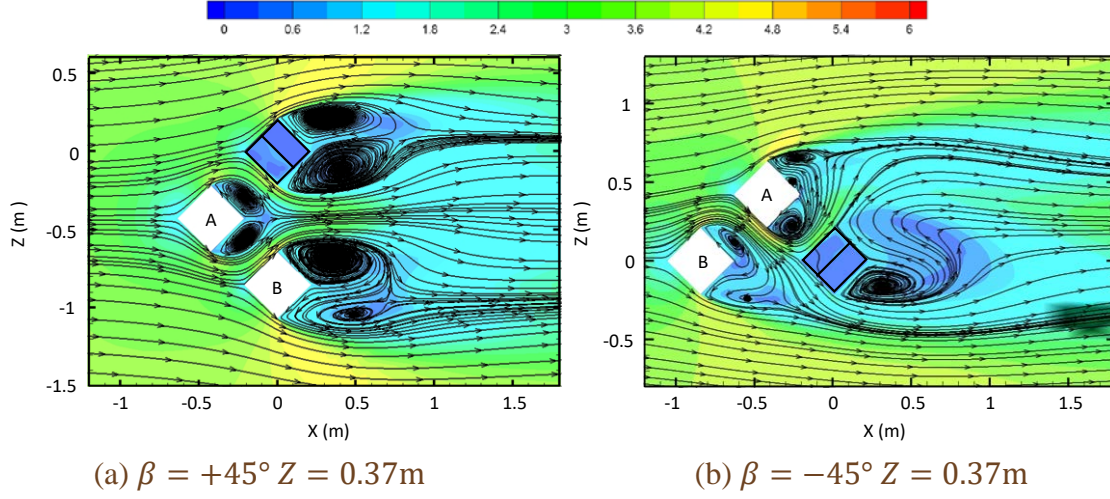


Figure 13. Streamlines and mean velocity on horizontal planes of the target building with oblique wind directions.

When the wind direction is oblique, the air flow patterns are significantly different. Figure 13(a) shows the airflow streamlines under the wind direction of $+45^\circ$ ($\beta = +45^\circ$). There are two windward and two leeward walls on each building, when the wind approaches, it first meets the sharp corners and then flows around the leeward side rapidly, which maintains the basic pattern on the building surfaces as that under the normal incident wind⁴². On the leeward side, the pressure difference leads to two low-pressure recirculation zones. With such flow pattern, the pollutant released from the windward units is quickly and effectively diluted into the flow stream while the two recirculation zones may induce that to re-enter into leeward units. The other wind direction ($\beta = -45^\circ$), as shown in Figure 13(b), with disparate airflow field, displays recirculation zones on both windward and leeward side

of the target building, which means more pollutant transportations may be brought on because of the two upstream interfering buildings.

Ventilation

Table 2 shows the ACH values for each unit under three wind directions. W represents a unit on windward side while L on the leeward side. When the wind direction is in normal incidence, the presence of upstream interfering buildings significantly improve the ACH values of windward side units, comparing to an isolated building²¹. However, when comparing the ACH values of units W1 and W2 found by the present study, to that of a single upstream building (W1 is 11.15 and W2 is 4.36)²⁴, ACH value of unit W1 was reduced to about 115%, which indicates that, with one more upstream interfering building (Building B), contaminants in unit W1 would have less chance to be transported outside from window. However, in unit W2, the ACH value would become increased by about 44%, this can be explained by the small vertex on the windward side of the target building which appears abreast unit W1. This near-wall wind fluctuation would drive indoor and outdoor air exchange in W2 but blocks in W1. On the leeward side, a negative effect can be noticed on ACH values comparing to that of an isolated building.

Table 2. ACH values of each unit under three wind directions.

ACH (h^{-1})	$\beta = 0$	$\beta = +45^\circ$	$\beta = -45^\circ$
W4	23.00	107.34	85.86
W3	4.92	107.55	90.47
W2	7.73	101.71	94.38
W1	5.19	93.16	101.28
L4	0.96	2.98	3.59
L3	0.94	13.88	11.37
L2	3.67	20.64	16.15
L1	4.06	20.05	14.48

When the wind directions are oblique ($\beta = +45^\circ$ & -45°), the ACH values of all units would become considerably larger than under normal incidence wind direction ($\beta = 0^\circ$). However, in both oblique wind directions, the unit L4 shows extremely low ACH value in comparison with other units. This may be caused by the low-pressure area on the leeward side of the target building which forms a relative low-speed zone adjacent to unit L4. The low air exchange rate of L4 may induce the concentration of air pollutant into the room.

From the present simulation results, the location of the unit has shown an obvious and essential impact on the characteristics of airflow. With the existence of two upstream interfering buildings, the interactions between indoor and outdoor airflow pattern would become redistributed, causing diverse wind directions and various routes of pollutant transmission.

The dispersion and re-entry tracer gas

Pollutants generated from one unit may re-enter into another unit of a multi-storey building under wind-induced natural ventilation in the urban environment. Especially for a densely populated city, like Hong Kong, most residential buildings are high-rise cylinder-like buildings, which leads to a high risk of pollutant transportations among units of windward and leeward sides. The pollutant transmission patterns are discussed in this section. Table 3 presents the re-entry ratio R_k of tracer gas from a source to other units under different wind directions. R_k equals 100%, means that the unit is the source location area (with a box in the table). The re-entry ratios equal or larger than 0.10% are highlighted. Elaborations of each case are presented below.

Table 3. Re-entry ratios R_k of each unit with diverse source locations under three wind directions.

R_k	$\beta = 0$	$\beta = +45^\circ$	$\beta = -45^\circ$	R_k	$\beta = 0$	$\beta = +45^\circ$	$\beta = -45^\circ$
W4	100.00%	100.00%	100.00%	W4	0.00%	0.00%	0.00%
W3	1.46%	0.00%	0.02%	W3	0.00%	0.00%	0.00%
W2	0.49%	0.00%	0.01%	W2	0.00%	0.00%	0.00%
W1	0.24%	0.00%	0.01%	W1	0.00%	0.00%	0.00%
L4	0.00%	0.00%	0.00%	L4	100.00%	100.00%	100.00%
L3	0.00%	0.01%	0.02%	L3	0.01%	0.16%	0.06%
L2	0.02%	0.01%	0.03%	L2	0.01%	0.22%	0.07%
L1	0.02%	0.01%	0.03%	L1	0.01%	0.20%	0.06%
W4	0.01%	0.00%	0.00%	W4	0.00%	0.00%	0.00%
W3	100.00%	100.00%	100.00%	W3	0.00%	0.00%	0.00%
W2	9.74%	0.00%	0.02%	W2	0.00%	0.00%	0.00%
W1	1.61%	0.00%	0.02%	W1	0.00%	0.00%	0.00%
L4	0.01%	0.00%	0.00%	L4	3.17%	0.79%	0.72%
L3	0.01%	0.01%	0.01%	L3	100.00%	100.00%	100.00%
L2	0.06%	0.02%	0.01%	L2	0.09%	0.04%	0.03%
L1	0.07%	0.02%	0.01%	L1	0.05%	0.03%	0.02%
W4	0.00%	0.00%	0.00%	W4	0.00%	0.00%	0.00%
W3	0.00%	0.00%	0.01%	W3	0.00%	0.00%	0.00%
W2	100.00%	100.00%	100.00%	W2	0.00%	0.00%	0.00%
W1	2.27%	0.00%	0.06%	W1	0.00%	0.00%	0.00%
L4	0.01%	0.00%	0.00%	L4	0.30%	0.15%	0.12%
L3	0.01%	0.02%	0.01%	L3	0.79%	2.76%	1.79%
L2	0.04%	0.03%	0.01%	L2	100.00%	100.00%	100.00%
L1	0.05%	0.03%	0.01%	L1	0.07%	0.03%	0.02%
W4	0.00%	0.00%	0.00%	W4	0.00%	0.00%	0.00%
W3	0.00%	0.00%	0.01%	W3	0.00%	0.00%	0.00%
W2	0.12%	0.00%	0.04%	W2	0.00%	0.00%	0.00%
W1	100.00%	100.00%	100.00%	W1	0.00%	0.00%	0.00%
L4	0.01%	0.00%	0.00%	L4	0.11%	0.03%	0.02%
L3	0.01%	0.02%	0.01%	L3	0.17%	0.19%	0.07%
L2	0.05%	0.03%	0.01%	L2	2.11%	1.44%	0.46%

L1	0.05%	0.04%	0.01%		L1	100.00%	100.00%	100.00%
----	-------	-------	-------	--	----	---------	---------	---------

Under normal wind direction ($\beta = 0^\circ$)

On the windward side, the exhaust air from units re-enters into leeward units with negligible ratios ($<0.1\%$). This basically demonstrates the generation of gaseous pollutants from the windward side, driven by the recirculation flows and large wind velocity on the lateral side, which directly disperse downstream. From the summary of re-entry ratios, more detailed observations can be made.

Firstly, when the gaseous pollutant is located in the unit W1, which is nearby the recirculation zone, R_k of most units are negligible, except for the minute value to W2 (0.12%). Obviously, the momentum of the downward flow is partially transferred to the frontal recirculation and partially to the lateral separations, as shown in Figure 9(b), which blocks the pollutant cross transmission.

Secondly, when the source is located in the unit W2, pollutants are mainly transported along the airflow to the unit below, as shown in Figure 9(b), due to the high pressure difference between the unit W2 area and the vortex below. The most affected unit is W1, which has the R_k value of 2.27%. This value is a significant reduction to that under the circumstance of a single upstream building, which is 15.16% as reported in Cui's work.²⁴ The result implies that, the presence of Building B would decrease R_k for unit W1, while also

decrease R_k of leeward units in the target building. This is because the vertical and horizontal recirculation zones would reduce the pollutant transmission, resulting from the increment increase of wind velocity in the lateral side of the target building. The dilute efficiency of gaseous contamination is amplified due to the presence of Building B.

Thirdly, when the pollutant is released from unit W3, the units below are both affected, especially for unit W2, R_k is up to 9.74%. Owing to the recirculation vortex behind the roof of Building A, the pollutants released from unit W3 are transported downward predominantly. Comparing to the circumstance of a single upstream building, a relative low air velocity area formed near the unit W2, would cause pollutants released from unit W3 to re-enter into W2 massively, larger than 6.76% as reported in Cui's work.²⁴ However, due to the recirculation vortex, R_k of unit W1 (1.61%) remains much less than Cui's work (8.32%).²⁴ This result can further illustrate that the existence of Building B could improve the dilution momentum of the tracer gas in unit W1.

Finally, when the pollutant source is located in unit W4, all windward units can be affected. Comparing to the results of Cui's work²⁴, the values of R_k beneath the source units are noticeably smaller, with 1.46%, 0.49% and 0.24% in present work to 5.52%, 3.92% and 6.46%, respectively, which are reduced over 73.5%. The reason for this reduction is likely to be the conflict between the dispersion and dilution momentums of the tracer gas with airflow complexity among building blocks. With the presence of Building B, the formation of

recirculation near ground and the asymmetric vortices on both sides of windows allows more tracer gas to disperse in lateral sides.

Generally, units on the windward side could be affected when the sources are located on the same side, and the room directly beneath the source unit should be included in the high-infection risk list in the event of a disease outbreak, even though the presence of Building B could reduce the possibility of pollutant inter-unit transmission to a large extent.

The phenomenon under two upstream buildings shows dissimilar results to that with a single upstream building when the source is located windward side. As shown in Cui's work²⁴, more pollutants released from windward side units re-enter into those of leeward. The relatively low re-entry ratios under two upstream buildings comparing to a single one can be explained. Because of the presence of Building B, wind velocity between building A and B, as shown in Figure 11(b), is much larger than that of a single upstream building, with the combined influence of recirculation down on the windward side, causing effective pollutant dilutions, reducing pollutants' transport into units on the leeward side.

Pollutants released from leeward side units show differentiable dispersion routes from the windward side. On the leeward side, the near-wall flow pattern is characterized by the combination of dominant upward flow and minute recirculation near ground. Due to the airflow pattern in such circumstance, pollutants are transported upward basically, which can be observed from the summary of re-entry ratios. When the source is located in unit L4, most

of the pollutant released, would be driven by the upward airflow, and become easily dispersed downstream and barely re-enter into other units. When pollutants are released from unit L1, L2 and L3, the tracer gas flows along the airflow patterns and re-enters into units above. The unit over the source unit has the largest value of R_k (up to 3.17%) comparing to others, which is most likely to become infected. R_k of units below source unit is negligible, as well as the units on the windward side.

Under oblique wind directions ($\beta = +45^\circ$ & -45°)

When the wind direction changes from normal to oblique incidence, R_k of most units decrease significantly due to the altered airflow pattern. All the windward pollutant transmissions are considered negligible under both oblique directions. This result is easily attained because of the relative large wind velocity on the windward side of the target building, as shown in Figure 13(a) and (b), which is in good agreement with that under the circumstance of a single upstream building²⁴. However, on the leeward side, recirculation zones are formed due to the pressure difference, which causes negative effects on pollutant transportation.

Under the wind direction of $+45^\circ$ ($\beta = +45^\circ$), two recirculation zones are formed on the leeward side of the target building, which leads to the complexity of airflow pattern. Pollutants are transported upward basically due to the wind pattern characterized by predominant upward airflow, except for the scenario of the source located in unit L4. When pollutants are released from unit L1, L2 and L3, the tracer gas flows along the airflow patterns

and re-enters into units above. However, when the pollutant is released from unit L4, all units below are affected non-negligibly. This is because that relative high wind velocity field and two vertices occur on the leeward side, which makes the pollutant more possible to re-enter into other units.

Under the wind direction of -45° ($\beta = -45^\circ$), a single recirculation zone is formed on the leeward side of the target building, which leads to comparatively simple airflow pattern. Pollutants are transported upward dominantly as the wind pattern characterized by main upward flow. When pollutants are released from unit L1, L2 and L3, the tracer gas disperses with the flow patterns and re-enters into units above, while when the pollutant is released from unit L4, the pollutants would become directly diluted downstream and do not re-enter into other units.

Inter-unit infectious risk assessment

The infectious risk between units can be evaluated by Equation (7) based on the Wells-Riley model⁷:

$$P = 1 - e^{\frac{-C_a I q p t}{Q}} \quad (7)$$

where q is the quanta generation rate, which represents the infectious source strength built upon both the emission rate and the infectivity of the pathogen⁴³, I represents the number of infectors, p represents the pulmonary ventilation rate of a person, t is the exposure time, Q is

the air flow rate for each unit, and C_d is the concentration decay coefficient, which equals to mass fraction of concentration (M_{i-j}). When a super infector is spreading in the target building, the inter-unit infectious risk can be very high, which is similar to that of the SARS outbreak in Hong Kong⁸. Assuming the infector exists in the unit, the quanta generation rate is 10,000 quanta per hour, the pulmonary ventilation of a person is $0.6m^3/h$, and the exposure time is $8h$. The inter-unit infectious risk evaluation is listed in Table 4. Colours are marked to different risk levels.

Table 4. Inter-unit infectious risk under different concentration decay coefficients.

Risk level	Concentration decay coefficient C_d	Inter-unit infectious probability P (%)
6	1	100
5	0.1	72.43
4	0.01	12.09
3	0.001	1.28
2	0.0001	0.13
1	0.00001	<0.13

Table 5 calculates the inter-unit infectious probability for each unit under different source locations and wind directions with colour marks. The infectious risks are in good agreement with re-entry ratio values. The infectious risks of all units are much smaller when the wind is in oblique incidence with sources located windward side, all results are under level 3, which can be considered negligible. However, under other circumstances, the inter-unit infectious risk can reach up to 99.99%. In this risk assessment, only one super infector is considered. If a second generation infection was produced in the target building, the infectious

risk could be increased essentially. Thus, the risk of inter-unit dispersion should not be neglected.

Table 5. Inter-unit infectious risks P of each unit with diverse source locations under three wind directions.

P	$\beta = 0$	$\beta = +45^\circ$	$\beta = -45^\circ$	P	$\beta = 0$	$\beta = +45^\circ$	$\beta = -45^\circ$
W4	100%	93.67%	96.83%	W4	0.00%	0.00%	0.00%
W3	58.44%	0.00%	0.07%	W3	0.00%	0.00%	0.00%
W2	17.01%	0.00%	0.03%	W2	0.00%	0.00%	0.00%
W1	12.66%	0.00%	0.03%	W1	0.00%	0.00%	0.01%
L4	1.35%	0.14%	0.36%	L4	100.00%	100.00%	100.00%
L3	1.54%	0.15%	0.43%	L3	4.55%	3.40%	1.52%
L2	1.62%	0.15%	0.48%	L2	1.17%	3.04%	1.35%
L1	1.60%	0.16%	0.53%	L1	1.04%	2.91%	1.28%
W4	0.10%	0.01%	0.01%	W4	0.00%	0.00%	0.00%
W3	100.00%	93.64%	96.22%	W3	0.00%	0.00%	0.00%
W2	97.61%	0.00%	0.07%	W2	0.00%	0.00%	0.00%
W1	60.17%	0.00%	0.07%	W1	0.00%	0.00%	0.00%
L4	3.71%	0.24%	0.19%	L4	99.99%	54.30%	44.71%
L3	4.41%	0.25%	0.23%	L3	100.00%	100.00%	100.00%
L2	4.82%	0.26%	0.26%	L2	6.76%	0.54%	0.46%
L1	4.82%	0.27%	0.29%	L1	3.72%	0.51%	0.42%
W4	0.02%	0.00%	0.01%	W4	0.00%	0.00%	0.00%
W3	0.09%	0.01%	0.03%	W3	0.00%	0.00%	0.00%
W2	100.00%	94.57%	95.67%	W2	0.00%	0.00%	0.00%
W1	72.62%	0.00%	0.17%	W1	0.00%	0.00%	0.00%
L4	2.67%	0.35%	0.15%	L4	60.09%	13.92%	9.07%
L3	3.21%	0.38%	0.18%	L3	91.88%	44.55%	37.29%
L2	3.56%	0.41%	0.20%	L2	100.00%	100.00%	100.00%
L1	3.58%	0.43%	0.22%	L1	4.81%	0.44%	0.38%
W4	0.02%	0.00%	0.01%	W4	0.00%	0.00%	0.00%

W3	0.10%	0.00%	0.02%	W3	0.00%	0.00%	0.00%
W2	4.64%	0.00%	0.13%	W2	0.00%	0.00%	0.00%
W1	100.00%	95.84%	94.64%	W1	0.02%	0.00%	0.00%
L4	2.88%	0.39%	0.14%	L4	29.12%	3.24%	1.65%
L3	3.43%	0.44%	0.17%	L3	42.43%	3.96%	1.87%
L2	3.76%	0.49%	0.19%	L2	81.75%	18.69%	8.12%
L1	3.74%	0.53%	0.21%	L1	100.00%	100.00%	100.00%

Discussion of re-entry ratio and infectious risk

The re-entry ratio R_k is a parameter which describes the amount of gaseous pollutants released from one unit into another. When the source is located in a specific unit, that the value R_k of another unit grows higher than others represents the total pollutants of this unit is larger. While the infectious risk P describes the possibility that people could become infected when exposing in a specific concentration of air pollutants. The probability people could become infected grows higher with the value of P . The re-entry ratio and infectious risk are two different parameters with separate focus points but related mathematically. By introducing air exchange rate (ACH), the relation can be written as Equation (8):

$$P = 1 - e^{\frac{-Iqpt}{V} \frac{(ACH)_i}{(ACH)_j} R_k} \quad (8)$$

where $(ACH)_i$ is the air exchange rate of the source unit i and $(ACH)_j$ is the re-entry unit j .

Some discussions can be made from the equation. Since the terms I, q, p, t and V are constants under a certain circumstance, the term $\frac{(ACH)_i}{(ACH)_j}$ affects the relation between P and R_k

essentially. When a pollutant source location is fixed, the $(ACH)_i$ is a determined value, which makes $(ACH)_j$ a key factor in this scenario. If the re-entry unit has smaller air exchange rate under same situation, people would become infected more easily. Taking the unit W3 as an example, when the source is located in unit W4, the R_k of unit W3 is 1.46% and the term $\frac{(ACH)_i}{(ACH)_j}$ is 467.03%. However, as the term $\frac{(ACH)_i}{(ACH)_j}$ is ranging from 100% (unit j has same air exchange rate with unit i) to extremely large (unit j has very small air exchange rate), the inter-unit infectious rate can vary from 17.15% to 100%.

In other words, the efficiency of natural ventilation of the re-entry unit could affect the infectious risk considerably. The infectious risk would increase while the ratio of air exchange rate of source unit with re-entry unit drops. Therefore, there is a need to consider re-entry ratio and infectious risk at same time when facing inter-unit dispersion problems.

Conclusions

Considering the influence of two upstream buildings, this study investigates the inter-unit dispersion around a multi-storey building using CFD method. Re-entry ratios of infectious agents between units were analysed and infectious risk was then assessed. Results were widely compared with previous studies that were based on an isolated building or a single upstream building. In general, the following conclusions were drawn from our findings.

The presence of upstream buildings does not necessarily deteriorate the wind environment around its downstream building. The airflow distribution could deviate greatly and could induce a relative low-speed area between upstream buildings and downstream building.

Under a normal incident wind, the addition of a second upstream building would only slightly vary the ACH values of the units of its downstream building. While under oblique wind directions, their presence would increase largely the ACH values of its downstream building.

When the wind direction is normal incidence, pollutants are dispersed mainly on the same side. The re-entry ratios from a unit to an opposite unit are very small which can be considered negligible, as well as the infectious risk. Comparing to a single upstream building, the presence of a second upstream building reduces the pollutant re-entry ratio R_k for most units when the source is located windward side, excluding a particular circumstance. While as sources are located on the leeward side, the re-entry ratios are not negligible comparing to the situation with a single upstream building, which is most likely to infect units immediately above the source units.

Under oblique wind directions, the main dispersion route of pollutants is altered from the windward side to the leeward side. The pollutants released from a windward unit disperse quickly to the outdoor wind flow and thus no obvious inter-unit dispersion occurs. However,

pollutants released from a leeward unit would transport upwards, where the units immediately above the source unit have the relatively high re-entry ratios. While the infectious risk shows the similar results.

This study reveals the inter-unit dispersion and infectious risk condition around a multi-storey building when considering the presence of two upstream buildings, which extends the existing understanding of inter-unit dispersions in built environments. However, restricted by computational resources, this study is still limited to a physical model with only three buildings. In addition, this study was performed in the framework of steady-state RANS modelling, which cannot reveal the transient characteristics of inter-unit dispersion. Improvements in these two aspects are expected in future studies.

Acknowledgement

This work was supported by a PhD studentship funded by Hong Kong Polytechnic University. The authors thank the anonymous reviewers and the editors for their useful comments.

Declaration

Authors' contribution:

All of the authors contributed in the preparation of this manuscript equally.

Conflict of interest:

The author(s) declared no potential conflicts of interest with respect to the research, authorship, and/or publication of this article.

References

1. Homod RZ, Sahari KSM. Energy savings by smart utilization of mechanical and natural ventilation for hybrid residential building model in passive climate. *Energy Build.* 2013;60:310-329.
2. Schulze T, Eicker U. Controlled natural ventilation for energy efficient buildings. *Energy Build.* 2013;56:221-332.
3. Tominaga Y, Stathopoulos T. Ten questions concerning modeling of near-field pollutant dispersion in the built environment. *Build Environ.* 2016;105:390-402.
4. Santos J, Mavroidis I, Reis N, Pagel E. Experimental investigation of outdoor and indoor mean concentrations and concentration fluctuations of pollutants. *Atmos Environ.* 2011;45(36):6534-6545.
5. ASHRAE. *ASHRAE handbook, fundamentals*. Atlanta, GA, American Society of Heating, Refrigerating and Air-conditioning Engineers, 2009.

6. Yu IT, Li Y, Wong TW, Tam W, Chan AT, Lee JH, Leung DY, Ho T. Evidence of airborne transmission of the severe acute respiratory syndrome virus. *N Engl J Med*. 2004;350(17):1731-1739.
7. Riley E, Murphy G, Riley R. Airborne spread of measles in a suburban elementary school. *Am J Epidemiol*. 1978;107(5):421-432.
8. Li Y, Duan S, Yu I, Wong T. Multi-zone modeling of probable SARS virus transmission by airflow between flats in Block E, Amoy Gardens. *Indoor Air* 2005;15(2):96-111.
9. Niu JL, Tung TCW. On-site quantification of re-entry ratio of ventilation exhausts in multi - family residential buildings and implications. *Indoor Air* 2008;18(1):12-26.
10. Liu XP, Niu JL, Kwok KCS, Wang JH, Li BZ. Investigation of indoor air pollutant dispersion and cross-contamination around a typical high-rise residential building: Wind tunnel tests. *Build Environ*. 2010;45(8):1769-1778.
11. Liu XP, Niu JL, Kwok KCS, Wang JH, Li BZ. Local characteristics of cross-unit contamination around high-rise building due to wind effect: mean concentration and infection risk assessment. *J Hazard Mater*. 2011;192(1):160-167.
12. Wang JH, Niu JL, Liu XP, Yu CWF. Assessment of pollutant dispersion in the re-entrance space of a high-rise residential building, using wind tunnel simulations. *Indoor Built Environ*. 2010;19(6):638-647.
13. Mu D, Shu C, Gao NP, Zhu T. Wind tunnel tests of inter-flat pollutant transmission characteristics in a rectangular multi-storey residential building, part B: Effect of source location. *Build Environ*. 2017;114:2812-2892.

14. Mu D, Gao NP, Zhu T. Wind tunnel tests of inter-flat pollutant transmission characteristics in a rectangular multi-storey residential building, part A: Effect of wind direction. *Build Environ*. 2016;108:159-170.
15. Chen QY. Ventilation performance prediction for buildings: A method overview and recent applications. *Build Environ*. 2009;44(4):848-858.
16. Van Hooff T, Blocken B. Coupled urban wind flow and indoor natural ventilation modelling on a high-resolution grid: A case study for the Amsterdam ArenA stadium. *Environ Model Softw*. 2010;25(1):51-65.
17. Ai ZT, Mak CM. Modeling of coupled urban wind flow and indoor air flow on a high-density near-wall mesh: Sensitivity analyses and case study for single-sided ventilation. *Environ Model Softw*. 2014;60:57-68.
18. Gao NP, Niu JL, Perino M, Heiselberg P. The airborne transmission of infection between flats in high-rise residential buildings: Tracer gas simulation. *Build Environ*. 2008;43(11):1805-1817.
19. Liu XP, Niu JL, Perino M, Heiselberg P. Numerical simulation of inter-flat air cross-contamination under the condition of single-sided natural ventilation. *J Build Perform Simul*. 2008;1(2):133-147.
20. Ai ZT, Mak CM, Niu JL. Numerical investigation of wind-induced airflow and interunit dispersion characteristics in multistory residential buildings. *Indoor Air* 2013;23(5):417-429.
21. Ai ZT, Mak CM. A study of interunit dispersion around multistory buildings with single-sided ventilation under different wind directions. *Atmos Environ*. 2014;88:1-13.

22. Ai ZT, Mak CM. Analysis of fluctuating characteristics of wind-induced airflow through a single opening using LES modeling and the tracer gas technique. *Build Environ.* 2014;80:249-258.
23. Ai ZT, Mak CM. Large eddy simulation of wind-induced interunit dispersion around multistory buildings. *Indoor Air* 2016;26(2):259-273.
24. Cui DJ, Mak CM, Kwok KCS, Ai ZT. CFD simulation of the effect of an upstream building on the inter-unit dispersion in a multi-story building in two wind directions. *J Wind Eng Ind Aerodyn.* 2016;150:31-41.
25. Launder BE, Spalding D. The numerical computation of turbulent flows. *Comput Methods Appl Mech Eng.* 1974;3(2):269-289.
26. Tsuchiya M, Murakami S, Mochida A, Kondo K, Ishida Y. Development of a new $k-\varepsilon$ model for flow and pressure fields around bluff body. *J Wind Eng Ind Aerodyn.* 1997;67:169-182.
27. Yakhot V, Orszag SA. Renormalization group analysis of turbulence. I. Basic theory. *J Sci Comput.* 1986;1(1):3-51.
28. Stathopoulos T. Computational wind engineering: Past achievements and future challenges. *J Wind Eng Ind Aerodyn.* 1997;67:509-532.
29. Yakhot V, Orszag S, Thangam S, Gatski T, Speziale C. Development of turbulence models for shear flows by a double expansion technique. *Phys Fluids A: Fluid Dynamics.* 1992;4(7):1510-1520.

30. Leitl B, Schatzmann M. Compilation of experimental data for validation purposes. *CEDVAL at Hamburg University*. <http://www.mi.uni-hamburg.de/cedval>. 1998.
31. Gorlé C, Van Beeck J, Rambaud P, Van Tendeloo G. CFD modelling of small particle dispersion: the influence of the turbulence kinetic energy in the atmospheric boundary layer. *Atmos Environ*. 2009;43(3):673-681.
32. Richard P, Hoxey R. Appropriate boundary conditions for computational wind engineering models using the k-e turbulence model. *J Wind Eng Ind Aerodyn*. 1993;46:145-153.
33. Ai ZT, Mak CM. CFD simulation of flow and dispersion around an isolated building: Effect of inhomogeneous ABL and near-wall treatment. *Atmos Environ*. 2013;77:568-578.
34. Fluent AF. 13.0 Theory Guide, Turbulence. *ANSYS Inc*, Canonsburg, PA. 2010.
35. Tominaga Y, Stathopoulos T. Turbulent Schmidt numbers for CFD analysis with various types of flowfield. *Atmos Environ*. 2007;41(37):8091-8099.
36. Blocken B, Stathopoulos T, Saathoff P, Wang X. Numerical evaluation of pollutant dispersion in the built environment: comparisons between models and experiments. *J Wind Eng Ind Aerodyn*. 2008;96(10):1817-1831.
37. Ai ZT, Mak CM. Potential use of reduced-scale models in CFD simulations to save numerical resources: Theoretical analysis and case study of flow around an isolated building. *J Wind Eng Ind Aerodyn*. 2014;134:25-29.

38. Franke J, Hellsten A, Schlunzen KH, Carissimo B. The COST 732 Best Practice Guideline for CFD simulation of flows in the urban environment: a summary. *Int J Environ Pollut*. 2011;44(1-4):419-427.
39. Meroney RN. Wind tunnel and numerical simulation of pollution dispersion: a hybrid approach. *Paper for Invited Lecture at the Croucher Advanced Study Institute, Hong Kong University of Science and Technology* 2004: 6-10.
40. Jiang Y, Alexander D, Jenkins H, Arthur R, Chen Q. Natural ventilation in buildings: measurement in a wind tunnel and numerical simulation with large-eddy simulation. *J Wind Eng Ind Aerodyn*. 2003;91(3):331-353.
41. Jiang Y, Chen QY. Buoyancy-driven single-sided natural ventilation in buildings with large openings. *Int J Heat Mass Transfer*. 2003;46(6):973-988.
42. Oke TR. *Boundary layer climates*. Routledge, London. 1978.
43. To S, Nam G. Risk assessment of infectious respiratory disease transmission in indoor environments. *Hong Kong University of Science and Technology, Hong Kong*, 2010.